Release and fate of nanoparticulate TiO2 UV filters from sunscreen: Effects of particle coating and formulation type

Danielle L Slomberg, Riccardo Catalano, Vincent Bartolomei, Jérôme Labille

Environmental Pollution 271 (2021) 116263

Contents lists available at ScienceDirect

Environmental Pollution

journal homepage: www.elsevier.com/locate/envpol

Release and fate of nanoparticulate TiO_2 UV filters from sunscreen: Effects of particle coating and formulation type☆

Danielle L. Slomberg*, Riccardo Catalano, Vincent Bartolomei, Jérôme Labille

Aix-Marseille University, CNRS, IRD, INRAe, Coll. France, CEREGE, Aix-en-Provence, France

ARTICLE INFO

Article history:
Received 24 September 2020
Received in revised form
7 December 2020
Accepted 8 December 2020
Available online 16 December 2020

Keywords:
Sunscreen UV filters
TiO_2 nanomaterials
Photocatalytic activity
Environmental fate
Aquatic pollution

ABSTRACT

Nanoparticulate mineral UV filters, such as titanium dioxide (TiO_2) nanocomposites, are being increasingly used in sunscreens as an alternative to organic UV filters. However, there is still a lack of understanding regarding their fate and behavior in aquatic environments and potential environmental impacts after being released from a bather's skin during recreational activities. In this work, we assessed the release, fate, and transformation of two commercial nanocomposite TiO_2 UV filters, one hydrophobic and one hydrophilic, in ultrapure water and simulated fresh- and seawater. The hydrophobic TiO_2 nanocomposite, T-SA, was coated with a primary Al_2O_3 photopassivation layer and a secondary stearic acid layer, while the hydrophilic TiO_2 nanocomposite, T-SiO_2, was coated with a single SiO_2 photopassivation layer. The influence of the sunscreen formulation was examined by dispersing the TiO_2 nanocomposites in their typical continuous phase (i.e., oil for T-SA and water for T-SiO_2) before introduction into the aqueous system. After 48 h of aqueous aging and 48 h of settling, 88–99% of the hydrophobic T-SA remained floating on top of the water column in all aqueous systems. On the other hand, 100% of the hydrophilic T-SiO_2 settled out of the water column in the fresh- and seawaters. With respect to the photopassivation coatings, no loss of the T-SA Al_2O_3 layer was detected after aqueous aging, but 99–100% dissolution of the SiO_2 layer on the T-SiO_2 nanocomposite was observed after 48 h in the fresh- and seawaters. This dissolution left behind T-SiO_2 by-products exhibiting a photocatalytic activity similar to that of bare rutile TiO_2. Overall, the results demonstrated that the TiO_2 surface coating and sunscreen formulation type drive environmental behavior and fate and that loss of the passivation layer can result in potentially harmful, photoactive by-products. These insights will help guide regulations and assist manufacturers in developing more environmentally safe sunscreens.

1. Introduction

Regulations on sunscreen UV filters continue to evolve, as concerns over potential adverse effects on human and environmental health are still emerging, especially with regard to organic (e.g., oxybenzone, octinoxate) UV filters (Narla and Lim, 2020; Rodríguez-Romero et al., 2019). Organic UV filters have already been shown to exhibit endocrine disrupting capabilities (Schlumpf et al., 2004), and the US Food and Drug Administration (FDA) has called for additional safety assessments of 12 common organic filters after recent studies demonstrated their systemic absorption in the human body following sunscreen application (U.S. Food and Drug Administration, 2019; Matta et al., 2019; Matta et al., 2020). Furthermore, several governments (e.g., US states of Hawaii and Florida (Key West), US Virgin Islands, Palau, Bonaire, Mexico) have approved legislation banning the sale of sunscreens containing oxybenzone and/or octinoxate due to their reported detrimental effects on aqueous environments and potential for bleaching of coral reefs (Schneider and Lim, 2019a; Balmer et al., 2005; DiNardo and Downs, 2018; Gago-Ferrero et al., 2012). Mineral UV filters, specifically titanium dioxide (TiO_2) and zinc oxide (ZnO), offer an alternative to organic UV filters, with the US FDA and European Scientific Committee on Consumer Safety (SCCS) authorizing their use in sunscreens at concentrations of up to 25% when applied to healthy skin (U.S. EPA, 2010; SCCS, 2012; SCCS, 2014). Both TiO_2 and ZnO are capable of reflecting and absorbing UV radiation, and while ZnO has a broad, flat absorption curve across the UVA-UVB spectrum, TiO_2 offers better UVB (290–320 nm) protection and a UVA (320–400 nm) protection that depends on particle size (Smijs and

☆ This paper has been recommended for acceptance by Bernd Nowack.
* Corresponding author.
E-mail address: slomberg@cerege.fr (D.L. Slomberg).

https://doi.org/10.1016/j.envpol.2020.116263

Pavel, 2011; Schneider and Lim, 2019b). However, the possible photocatalytic activity, toxicity, and environmental fate and impact of these approved mineral UV filters still require further investigation, particularly for the nanoparticulate forms (Labille et al., 2020a; Hanigan et al., 2018).

Nanoparticulate TiO_2 UV filters are already used in many commercial sunscreens due to their improved sun protection and aesthetics compared to their micron-sized counterparts. While effective at UV absorption, TiO_2 is also known for its photocatalytic properties. Under UV radiation, TiO_2 can generate reactive oxygen species (ROS) such as •OH, $^1O_2$, and $O_2^{\bullet-}$, which are capable of degrading organic molecules and may also damage skin and even environmental biota (Li et al., 2012; Sendra et al., 2017a; Sendra et al., 2017b; Kumar and Bansal, 2013). For this reason, the less photocatalytic rutile TiO_2 form is preferred over the highly photocatalytic anatase form in cosmetic formulations (Fujishima et al., 2008). To further prevent unwanted photo-induced reactions and protect the consumer's skin, the rutile TiO_2 core is commonly coated with an inert mineral layer (e.g., Al_2O_3 or SiO_2) (Jang et al., 2016; King et al., 2008). A second coating (e.g., polydimethylsiloxane (PDMS), stearic acid) may also be added to the TiO_2 nanocomposite to enhance the UV filter dispersion in the sunscreen, depending on the type of formulation (Auffan et al., 2010; Catalano et al., 2020a). Hydrophilic UV filters are preferentially dispersed in the sunscreen water phase, while those that are hydrophobic favor the oil phase (Faure et al., 2013; Semenzato et al., 1994). Moreover, sunscreen manufacturers use either an oil-in-water or water-in-oil emulsion in order to achieve the desired texture, feel, and water resistance of the formulation, and it is reasonable to expect that they may exhibit contrasting environmental fates. Thus, consideration of the sunscreen formulation type as well as the TiO_2 particle coating will be crucial for assessing the environmental impacts of nanoparticulate UV filters, as the various sunscreen components (e.g., oils, emulsifying agents, thickeners) may influence their release, behavior, and fate in aqueous environments (Tovar-Sánchez et al., 2019; Catalano et al., 2020b).

Several researchers have already investigated the real-time occurrence of sunscreen TiO_2 UV filters in fresh- and seawaters during recreational activity (Gondikas et al., 2014; Reed et al., 2017; Tovar-Sánchez et al., 2013; Labille et al., 2020b; Gondikas et al., 2018; Rand et al., 2020). Increases in Ti-containing particles in freshwaters were observed during the summer season, indicating TiO_2 UV filter inputs at μg/L concentrations (Gondikas et al., 2014; Reed et al., 2017; Gondikas et al., 2018). Overall, these studies suggest that TiO_2 UV filters released into freshwaters have a rather short residence time (i.e., hours to a few days) in the water column before agglomerating and sedimenting due to the presence of cations in the natural waters that reduce electrostatic repulsions between particles, although TiO_2 UV filter behavior will also be dependent on environmental conditions (e.g., hydrological changes) (Rand et al., 2020; Botta et al., 2011). On the other hand, TiO_2 UV filters released into seawaters were concentrated in the top surface layer at 38–900 μg/L Ti (Tovar-Sánchez et al., 2013; Labille et al., 2020b), likely due to associations with hydrophobic sunscreen components remaining at the air-water interface. While recent analytical developments have improved our ability to detect and differentiate anthropogenic particles from natural colloids in fresh- and seawaters (Gondikas et al., 2018; Loosli et al., 2019; Slomberg et al., 2020a), knowledge on the environmental fate and persistence of nanoparticulate TiO_2 UV filters released from sunscreens during recreational activity is still lacking.

Fundamental questions remain to be addressed regarding the release of nanoparticulate TiO_2 UV filters into natural aqueous systems, including their residence time in the water column with relation to surface coating and sunscreen formulation type, any transformation and loss of their photopassivation coating, and how the aged residues may impact environmental biota. In response, the aims of our study were (1) to evaluate the dispersion of two different commercial nanoparticulate TiO_2 UV filters, one hydrophobic and one hydrophilic, into simulated fresh- and seawater; (2) to determine the stability and fate of these nanoparticles in the water column; (3) to evaluate the resistance of the corresponding photopassivation layer to aqueous aging; and (4) to assess the potential for ROS generation from the aged nanoparticulate by-products. Of note, since a hydrophobic and a hydrophilic UV filter were compared here, different protocols were adapted based on their respective behaviors to answer these questions. Through these investigations, our goal was to further evaluate the potential environmental impacts of nanoparticulate TiO_2 UV filters and their use as an alternative, and provide key data necessary for guiding the development of safe(r)-by-design sunscreens and consumer products (Labille et al., 2020a).

2. Materials and methods

2.1. Preliminary dispersion test of commercial sunscreens

The propensity for a commercial sunscreen to disperse in the aqueous environment cannot be predicted from the information on the label, as it does not reflect the type of emulsion. To evaluate the character of sunscreens containing TiO_2 UV filters, we assessed the dispersion of four commercial sunscreens in both water and ethanol. Well-known brands currently on the European market (i.e., Nivea Sun, Mixa, Avène, and Acorelle) with high sun protection factor (SPF) values (SPF $\geq$50) were selected for this test. The experimental details and images of the resulting dispersions are given in Supplementary Material Experimental S1 and Figure S1, respectively. We assumed that sunscreens that dispersed well in water were oil-in-water emulsions, while those that dispersed only in ethanol were water-in-oil emulsions. Of the four tested sunscreens, two dispersed only in water and the other two dispersed only in ethanol. As this test was limited to only four commercial products, these results cannot be used to provide a statistical representation of emulsion types on the market. Nevertheless, it confirmed that both emulsion types are present on the market and that their contrasting behaviors must be accounted for when assessing sunscreen environmental fate.

2.2. Commercial nanoparticulate TiO_2 UV filter characterization

Two different nanoparticulate TiO_2 UV filters commercially available from Merck, one hydrophobic and one hydrophilic, were provided as dry powder samples by the manufacturer for this study. The hydrophobic filter, Eusolex® T-S, here referred to as T-SA, is composed of a rutile TiO_2 core, coated with a primary Al_2O_3 protective layer and a secondary stearic acid layer. The hydrophilic UV filter, Eusolex® T-AVO, here referred to as T-SiO_2, is also composed of a rutile TiO_2 core and is coated with a SiO_2 protective layer. These nanoparticulate TiO_2 UV filters were selected based on their continued presence on the market, their use as reference materials in several previous studies (Couteau et al., 2008; Lewicka et al., 2011; Lewicka et al., 2013; Couteau and Coiffard, 2015), and their similarity to TiO_2 UV filters evaluated by the European SCCS (SCCS, 2014).

To verify the elemental compositions of the T-SA and T-SiO_2 nanoparticles (NPs), 300 mg of the powder was heated stepwise to 920 °C. The percent composition of organic matter was determined by loss on ignition. A conventional tetraborate alkaline fusion was

then performed on the heated residues, followed by analysis with inductively coupled plasma-atomic emission spectroscopy (ICP-AES, PerkinElmer 4300 DV) to determine Ti (336.121 nm), Al (396.152 nm), and Si (251.611 nm) concentrations which were then converted to % TiO_2, Al_2O_3, and SiO_2. Details on the loss on ignition and alkaline fusion procedures can be found in Supplementary Material Experimental S2.

The rutile mineralogy and crystallite size of the particles were confirmed by X-ray diffraction (XRD) using a PANalytical X'Pert PRO (Limeil-Brevannes, France). Size and morphology of the particles were evaluated with dynamic light scattering (DLS, Zetasizer Nano ZS, Malvern) and a Hitachi SU 9000 Ultra-high Resolution scanning electron microscope (SEM). For size evaluation using DLS, the nanoparticulate UV filters were dispersed in their typical sunscreen phase (i.e., oil for the hydrophobic T-SA and ultrapure water for the hydrophilic T-SiO_2). The oil phase, a mixture of commercial emollients and an emulsifier (containing an alkylpolyxyloside and polymer surfactant), consisted of a 2:2:1 ratio of Tegosoft® P (Evonik), Cetiol® LC (BASF), and Easynov (SEPPIC™), respectively (Catalano et al., 2020a). The zeta potential of the T-SiO_2 particles was also measured with the Zetasizer Nano ZS in a 1 mM NaCl solution at pH 7.4.

2.3. Aqueous solutions

All synthetic solutions were prepared with ultrapure water (Merck-Millipore, Milli-Q® purification system, ≥18.2 MΩ-cm, TOC ≤ 3 ppb, ionic strength < 0.02 mM) unless otherwise noted. The simulated freshwater and seawater used in this study were the commercially-available Cristaline® (Source de la Doye, pH 7.5, ionic strength ~5.8 mM) and Instant Ocean® artificial seawater (pH 8.2, ionic strength ~575 mM), respectively (Slomberg et al., 2020b). To evaluate the potential effects of pH and salinity on NP aging, ultrapure water was adjusted to pH 8 using 1 mM $NaHCO_3$.

2.4. Aging of nanoparticulate TiO_2 UV filters in aqueous solution

Before aqueous aging, the T-SA or T-SiO_2 NPs were first dispersed in their respective oil (i.e., mixture of emollients and emulsifier previously described) or water sunscreen phase at 50 g/L to represent a typical sunscreen containing 5% TiO_2 and magnetically stirred overnight (500 rpm) (Botta et al., 2011). Of note, maximum NP dispersion was achieved at 500 rpm, as additional increases in agitation speed and sonication did not further reduce the NP size distribution. The aging was then performed by injecting 2 mL of the TiO_2 NP suspension into either 248 mL of ultrapure water, freshwater (Cristaline®), or artificial seawater (Instant Ocean®) for a NP concentration of 400 mg/L in each system. This NP concentration was selected to represent a maximum localized release scenario during recreational activity for one bather after whole-body application of ~16 g of a 5% TiO_2 sunscreen (Ficheux et al., 2016) and ensure sufficient material for analysis based on previous work (Labille et al., 2010). The suspensions were magnetically stirred (300 rpm) over 48 h under artificial daylight (HQI-BT lamp OSRAM, E40, 400 W, irradiance = 0.8 mW/cm^2) (Ramalho et al., 2002). Using this artificial daylight source, the daily dose of ~69 J/cm^2 was similar to the average daily personal exposure (~50 J/cm^2) previously reported by Romanhole et al. (2016) Aqueous aging was also performed in the dark under the same conditions by covering the reaction flasks with aluminum foil. For the samples aged under artificial daylight, an appropriate volume of ultrapure water was added after 6, 24, and 48 h of aging to compensate for any evaporation. The temperature was monitored for all samples and remained between 21 and 23 °C over the course of the experiment. Blank samples (i.e., ultrapure, freshwater, and seawater without added TiO_2 NPs) were also aged under the same conditions.

2.5. Dispersion and fate of nanoparticulate TiO_2 UV filters

Samples (10 mL) of each aqueous phase were collected from the center of the reaction flask while stirring at 30 min, 3 h, 6 h, 24 h, and 48 h to evaluate the presence of the TiO_2 NPs in the aqueous phase over time via elemental analysis. Additionally, laser diffraction (Mastersizer 3000, Malvern) measurements were immediately performed on each T-SiO_2 sample to investigate the particle size distribution over time. Of note, the size distribution of T-SA NPs in the aqueous phase was not determined using laser diffraction due to the inability to completely distinguish the NPs apart from emulsified oil droplets. After 48 h of sample aging, the agitation was stopped and the aged TiO_2 by-products were allowed to settle for 48 h in the reaction flask.

Once the 48 h settling time was complete, the top oil surface layer (T-SA samples only), the aqueous (colloidal) phase, and the sediment were separated to determine the fate of the TiO_2 NPs. The top oil surface layer (~0.25 cm) was gently removed where applicable, followed by the aqueous phase. The aged by-products in the sediment were then collected via a centrifugation and wash procedure. The sedimented T-SA particles were separated from other oil phase components by extraction with hexanes, then washed twice with absolute ethanol (1 h, 2675*g*) and dried. The sedimented T-SiO_2 particles were washed twice with absolute ethanol (1 h, 2675*g*) and dried. All liquid and solid samples were subjected to total decomposition using microwave-assisted acid digestion (UltraWAVEmicrowave acid digestion system, Milestone Inc.) before being analyzed for Ti content by ICP-AES. Details on the acid digestion procedure can be found in Supplementary Material Experimental S3. This data was used in combination with the elemental compositions to calculate the % NP in each compartment relative to the amount of NP injected. The % T-SA NP remaining in the top oil surface layer was estimated by subtracting the amount of T-SA NP in the aqueous phase and sediment from the initial amount injected.

2.6. Evaluation of coating stability

Degradation of the Al_2O_3 and SiO_2 protective layers of the T-SA and T-SiO_2 NPs, respectively, was monitored by analyzing the concentration of Al or Si species (<2 nm) released into the waters during the aging process. Aliquots (4 mL) of the aqueous phase were recovered at 3 h, 6 h, 24 h, and 48 h and centrifuged with Amicon® Ultra-4 10 K centrifugal filter devices (10 000 MWCO, size retention limit ~ 2 nm, Merck-Millipore) at 4000*g* for 1 h to separate the aged TiO_2 NPs from the solution. The recovered filtrates were then analyzed for Al or Si with ICP-AES as an indication of degradation and loss of the protective photopassivation layer. Having already shown in Slomberg et al. (2020b) that dissolution of the SiO_2 protective layer on the T-SiO_2 particles is possible during aqueous aging, we sought to further understand the kinetics of the coating degradation and the effects of pH and ionic strength. Thus, the concentration of released Si species was also measured in ultrapure water with no pH adjustment (pH ~6), ultrapure water adjusted to pH 8 (1 mM $NaHCO_3$), and freshwater (pH 7.5, ionic strength ~5.8 mM) over 7 days in the dark, with aliquots taken at 1, 3, 5, and 7 days.

The effects of degradation on particle surface charge were also investigated by measuring the zeta potential of the T-SiO_2 by-products after aging in ultrapure water, freshwater, and seawater. The aged T-SiO_2 NPs recovered in the aqueous phase or the sediment after 48 h aging and 48 h settling were re-suspended in 1 mM

NaCl (100 mg/L), the pH was adjusted to pH 2, 4, or 6 with HCl, and the zeta potential was measured using a Malvern Zetasizer Nano ZS. Zeta potentials of the pristine T-SiO_2 and the TiO_2 core (recovered after complete dissolution of the SiO_2 layer at pH 13 for 5 days) were also evaluated as a reference.

2.7. Photocatalytic activity of aged nanoparticulate T-SiO_2

A rhodamine degradation test was performed to provide insight on the potential for the aged T-SiO_2 particles to form ROS upon exposure to daylight (Aarthi and Madras, 2007). Rhodamine organic dyes (e.g., rhodamine 6G, rhodamine B) have a high molar absorptivity in the visible spectrum, however in the presence of ROS, the rhodamine molecules can be degraded, no longer capable of absorbing light. Thus, a decrease in rhodamine concentration (compared to controls) in the presence of TiO_2 and under daylight conditions is associated with ROS generation. Of note, as this test requires the complete dispersion of the NPs in the aqueous phase, only the hydrophilic T-SiO_2 particles (i.e., pristine and freshwater-aged) were evaluated. The freshwater-aged T-SiO_2 particles tested here were those recovered after 48 h of aging under daylight and 48 h of settling, followed by washing with ethanol and drying. As a comparison, rhodamine (Rhodamine 6G, Sigma-Aldrich) degradation was also analyzed in the presence of two commercial references, the highly photocatalytic Evonik P25 TiO_2 NPs (80% anatase, 20% rutile, 25 nm) and the less photoreactive 100% rutile NanoAmor TiO_2 NPs (5–30 nm). Briefly, the TiO_2 particles (25 mg/L TiO_2) were first dispersed in ultrapure water with 2.5 mg/L rhodamine and allowed to equilibrate in the dark for 30 min under stirring (500 rpm) to account for any rhodamine adsorption to the particle surface. After this equilibration time, aliquots were removed to determine the rhodamine present in solution at the 0 min time point, just before exposing the samples to artificial daylight. To begin the rhodamine degradation test, the samples were then stirred (500 rpm) under artificial daylight (HQI-BT lamp OSRAM, E40, 400 W, irradiance = 0.8 mW/cm^2) with aliquots removed at 90, 180, and 240 min. The collected samples were immediately centrifuged (6000 rpm, 10 min) to separate the TiO_2 NPs from the supernatant and the UV–visible absorbance of the supernatant was measured from 190 to 600 nm with a JASCO V-650 UV–Vis spectrophotometer. The rhodamine C/C_0 was calculated at each time point using the rhodamine maximum absorbance peak at 528 nm.

3. Results and discussion

3.1. T-SA and T-SiO_2 nanocomposites exhibit contrasting properties

The two nanoparticulate TiO_2 UV filters, both produced by the same manufacturer, were composed of ~80 wt% TiO_2, confirmed to be rutile with XRD (Supplementary Material Fig. S2). In agreement with the composition reported by the manufacturer, the T-SA primary protective layer consisted of 7.8 ± 0.4 wt% Al_2O_3 and the secondary organic (i.e., stearic acid) layer represented 15.6 ± 0.2 wt % of the nanocomposite. As expected, the protective layer of the T-SiO_2 NPs was composed of 16.8 ± 0.1 wt% SiO_2 (Slomberg et al., 2020b). However, the loss on ignition analysis also revealed the presence of organic material (3.6 ± 0.7 wt%) on the T-SiO_2 nanocomposite surface, possibly a contamination from manufacturing processes. With scanning electron microscopy (SEM), the T-SA and T-SiO_2 nanocomposites were shown to be of similar width (i.e., 15–20 nm), but the T-SA NPs were slightly longer at 60–100 nm versus 30–80 nm for the T-SiO_2 (Supplementary Material Fig. S3). The crystallite sizes of the T-SA and T-SiO_2 NPs determined with XRD were 11.4 and 19.2 nm, respectively. When dispersed in their respective sunscreen phase (i.e., oil for T-SA and water for T-SiO_2), the NPs exhibited differences in hydrodynamic size and dispersion. As previously detailed by Catalano et al. (2020a), although the hydrophobic T-SA was dispersed in an oil phase, the size distribution was bi-modal with peaks at 282 and 1373 nm, indicating the presence of aggregates. On the other hand, the T-SiO_2 was well-dispersed in the ultrapure water, with a main peak size of 353 nm. The hydrophilic T-SiO_2 nanocomposites had a zeta potential of −38.3 ± 0.5 mV (pH 7.4, 1 mM NaCl), resulting in electrostatic repulsion between the T-SiO_2 NPs in the water phase, and leading to improved dispersion. Indeed, silica surfaces are known to exhibit a highly negative surface charge due to the presence of surface silanol groups, with a zeta potential of −35 to −50 mV between pH 6 and pH 10 (Metin et al., 2011). A summary of these physico-chemical characterization data can be found in Supplementary Material Table S1. Overall, the similar rutile TiO_2 core composition and comparable sizes of the T-SA and T-SiO_2 nanocomposites made it possible to effectively study the influence of the hydrophobic and hydrophilic surface properties on the nanocomposite fate and behavior in aqueous environments.

3.2. Hydrophobic and hydrophilic TiO_2 UV filters follow different fate scenarios in water column

Fig. 1A shows the compartmentalization of the T-SA and T-SiO_2 NPs between the top oil surface layer (T-SA only), the aqueous (colloidal) phase, and the sediment after 48 h of aging under daylight and 48 h of settling in either ultrapure, freshwater, or seawater. The T-SA NPs did not readily enter the water column, with 91.8, 88.4, and 99.9% remaining in the oil surface layer that formed on top of the ultrapure, freshwater, and seawater phases, respectively. A small percentage of hydrophobic T-SA (1.4–1.6%) remained in the aqueous phase in the ultrapure water and freshwater systems. Furthermore, 6.8 and 10.0% of the injected T-SA NPs were recovered in the sediments of the ultrapure water and freshwater systems, respectively, demonstrating that the majority of the T-SA entering the aqueous phase was unstable. Due to the presence of emollients and an emulsifier in the sunscreen oil phase, the hydrophobic T-SA NPs were able to enter the ultrapure and freshwaters through emulsified oil droplets, creating an oil-in-water emulsion (Marti-Mestres et al., 1997). Once the agitation was stopped after 48 h of aging and the systems were allowed to settle, the fate of the emulsified T-SA-containing oil droplets was likely governed by a combination of coalescence and sedimentation phenomena. Coalescence of the T-SA containing oil droplets could result in the transfer of the T-SA NPs back into the top oil layer (André et al., 2003). On the other hand, the T-SA containing oil droplets could also agglomerate and sediment, as a result of charge neutralization and/or hydrophobic interactions between the emulsifier components, emollients, and T-SA NPs (Loosli and Stoll, 2017; Skoglund et al., 2013). In the seawater system, minimal T-SA (<1%) was detected in the aqueous phase and sediment, suggesting that the T-SA NPs were not able to readily enter the seawater through emulsified oil droplets. Indeed, repulsive electrostatic interactions at the oil-water interface have been shown to increase with salinity, and the seawater used here had an ionic strength of ~575 mM, 100× greater than that of the freshwater (Park et al., 2008).

In contrast, the hydrophilic T-SiO_2 NPs completely dispersed into each of the three aqueous phases (i.e., ultrapure, freshwater, seawater), yet after the 48 h of aging and 48 h of settling, differences in dispersion stability were observed depending on the water type (Fig. 1A). The Ti elemental analysis results revealed that 43% of the T-SiO_2 NPs were stable in the ultrapure water, while the other 57% had sedimented. The highly negative charge of the silica

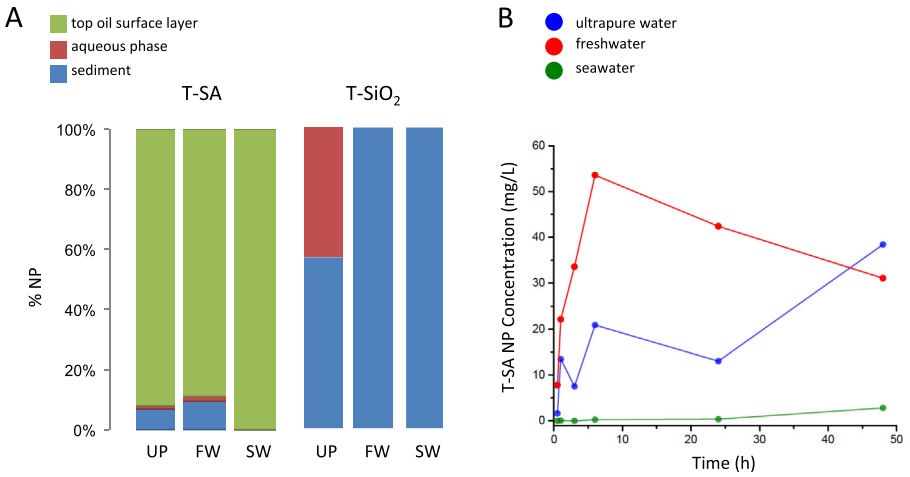

Fig. 1. (A) Percent of T-SA and T-SiO_2 particles in top oil surface layer, aqueous phase (colloidal), and sediment after 48 h aqueous aging under daylight and 48 h settling in ultrapure water (UP), freshwater (FW), and seawater (SW). (B) Kinetics of T-SA NP dispersion into aqueous phase over time under daylight conditions.

surface at the pH of ultrapure water (pH ~ 6) (Metin et al., 2011), and electrostatic repulsions should have resulted in stability of the dispersion. However, some T-SiO_2 homo-aggregation and sedimentation still occurred, likely due to aggregates present in the initial suspension. In the freshwater (0.5 mM NaCl, 1.6 mM $CaCl_2$) and seawater (400 mM NaCl, 8 mM $CaCl_2$), the T-SiO_2 NPs were not stable in the water column, with complete sedimentation observed after 48 h of settling. As previously demonstrated for both SiO_2 and TiO_2 NPs (Praetorius et al., 2014; Keller et al., 2010; Topuz et al., 2014; Thiagarajan et al., 2019), the cations (e.g., Na^+, Ca^{2+}) present in these abiotic aqueous systems were capable of shielding the NP negative surface charge, thus reducing electrostatic repulsions and promoting homo-aggregation and sedimentation. However, it should be noted that at high NaCl concentrations (e.g., 200–500 mM), such as those in seawater, the TiO_2 NPs can rapidly form large, but loosely suspended homo-aggregates that may remain suspended and mobile in the environment for several minutes (e.g., 45 min) before sedimenting (Hsiung et al., 2016). Altogether, the results shown in Fig. 1A suggest that in natural aqueous environments (e.g., fresh and seawater) the T-SA NPs will tend to remain floating on top of the water column, while the T-SiO_2 NPs will sediment. This behavior was not related to the presence of daylight, as the same trends were observed for the T-SA and T-SiO_2 allowed to age and settle in the dark (Supplementary Material Fig. S4).

To better understand the final fate scenario of the NPs in the different phases presented in Fig. 1A, the state of T-SA and T-SiO_2 NP dispersion in the aqueous phase was investigated over the 48 h of aging leading up to the 48 h settling period. Although the majority (88–99%) of the T-SA NPs remained in the top oil layer after 48 h of aging and 48 h of settling, the kinetics of T-SA NP dispersion into the aqueous phase during aging under daylight conditions was monitored at 30 min, 3 h, 6 h, 24 h, and 48 h to provide further insight into T-SA behavior in aqueous environments (Fig. 1B). The largest amount of T-SA NP transfer into the aqueous phase was noted for the freshwater system, with 53.6 mg/L T-SA NP detected after 6 h of aging. This concentration represented 17.4% of the total T-SA NP amount injected into the system (~309 mg/L) as determined using elemental analysis. In the ultrapure water, transfer of the T-SA NPs into the aqueous phase from the top oil layer was slower and the maximum concentration of ~38.5 mg/L T-SA NP (12.5% of T-SA injected) was not observed until 48 h of aging. The transfer of T-SA NPs into the seawater was even lower, as expected based on the results from Fig. 1A, with only 0.9% of the injected T-SA (2.8 mg/L T-SA NP) present in the aqueous phase after 48 h. As previously stated, the T-SA NPs can enter the ultrapure water and freshwater through emulsified oil droplets. The faster dispersion kinetics of the emulsified T-SA containing oil droplets into the freshwater compared to the ultrapure water seen here is likely related to oil droplet formation and stability as a function of salinity. For example, previous studies have demonstrated the enhanced formation and electrostatic stabilization of polymer-surfactant complexes (i.e., emulsified oil droplets) in water after the addition of up to 100 mM monovalent salts (André et al., 2003; Binks et al., 2006; Mya et al., 2003; Fundin et al., 1996). Furthermore, the aqueous phase T-SA NP concentrations at 48 h of aging, just before the agitation was stopped, compared to the T-SA NP fate in the different compartments (i.e., top oil layer, aqueous, sediment) after 48 h of settling, provided insight as to the tendency of the T-SA NP containing oil droplets toward coalescence back into the top oil layer or toward aggregation and sedimentation. After 48 h of aging in the ultrapure water system, 9.6 mg of T-SA were present in the aqueous phase, however, after 48 h of settling, only 6.2 mg T-SA were recovered in the aqueous phase and the sediment, suggesting that ~35% of the T-SA coalesced back into the top oil layer. Conversely, none of the 7.8 mg T-SA present in the freshwater system at 48 h coalesced back into the top oil layer, with the majority of the T-SA containing oil droplets aggregating and sedimenting. In the seawater, 95% of the 0.7 mg T-SA present at 48 h coalesced back into the oil layer after settling. Therefore, these results demonstrate the crucial role that salinity plays in the dispersion as well as final fate of the hydrophobic T-SA NPs. Similar trends were also observed for T-SA NPs aged in the dark (Supplementary Material Figure S5).

On the other hand, the hydrophilic T-SiO_2 NPs easily and completely dispersed in all three of the aqueous systems. To gain further understanding as to the aggregation state of the T-SiO_2 NPs, the volume-based size distribution was measured after 30 min of aging in the ultrapure water, freshwater, and seawater under daylight conditions using laser diffraction (Fig. 2). The T-SiO_2 size distributions were multi-modal in all of the aqueous systems, but freely-dispersed, non-aggregated nanoparticles were only present in the ultrapure water, as illustrated by the prominent peak centered around 0.15 μm. A significant contribution of small T-SiO_2 aggregates between ~0.2 and 1 μm was also observed. Due to the presence of cations in the freshwater and seawater and their ability

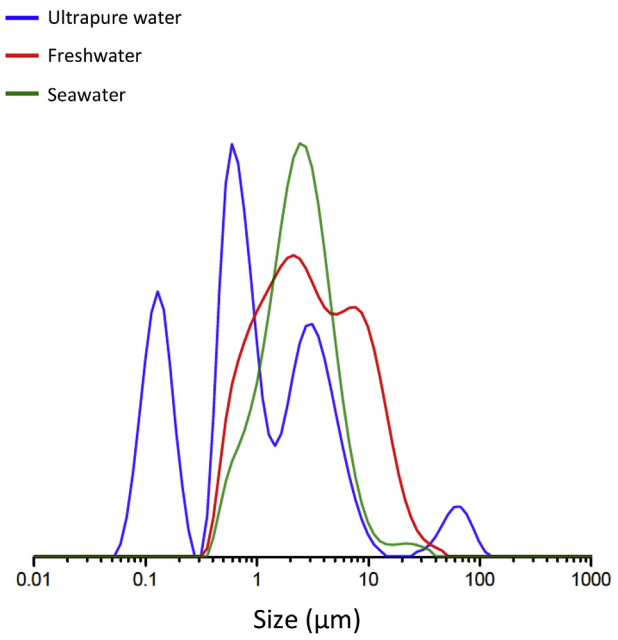

Fig. 2. T-SiO_2 volume-based size distribution in ultrapure (blue), freshwater (red), and seawater (green) after 30 min under light conditions. (For interpretation of the references to colour in this figure legend, the reader is referred to the Web version of this article.)

to screen the NP negative surface charge, the T-SiO_2 NPs formed large (>1 μm) homo-aggregates. No further changes in the T-SiO_2 size distributions were observed over the 48 h duration of aging (data not shown). The presence of both freely-dispersed and aggregated T-SiO_2 NPs in the ultrapure water after aging explains their contrasting fates in the aqueous phase (43%) versus the sediment (57%) after the 48 h of settling. The influence of T-SiO_2 aggregation state was even more evident in the freshwater and seawater systems, where the presence of only larger aggregates led to 100% sedimentation after 48 h of settling. Thus, in natural aqueous environments, the T-SiO_2 NPs will either homo-aggregate (assuming a high localized concentration) or hetero-aggregate with natural suspended matter and settle out of the water column.

3.3. Estimated TiO_2 mass flow from a single bather can vary with particle coating

The environmental implications of these contrasting fate scenarios were considered by estimating the mass flow of nanoparticulate TiO_2 UV filters released into an aqueous environment from one bather after sunscreen application. Taking into account the whole-body application of ~16 g of a 5% TiO_2 sunscreen, and a 50% skin retention factor, 400 mg of TiO_2 would be locally released per bather (Botta et al., 2011; Ficheux et al., 2016; Danovaro et al., 2008). Fig. 3 shows how this mass of TiO_2 would then be distributed between the top surface layer, the water column, and the sediment.

The majority of the hydrophobic T-SA NP UV filters were shown to remain stable in the sunscreen oil phase, floating at the air-water interface. As shown in Fig. 3, 42 mg of the 400 mg of hydrophobic TiO_2 NPs leaving the bather's skin may enter the aqueous phase in freshwater conditions, but in seawater that mass would only be 4 mg due to the increased salinity. Concerning the final fate of these hydrophobic NPs, 40 mg would be deposited in the freshwater sediment, but in seawater the original 400 mg would remain floating in the top surface layer at the air-water interface. This UV filter fate in the water top surface layer also implies a higher local NP concentration. Indeed, the temporary accumulation of TiO_2 UV filters at the air-water interface has already been observed in field samples from recreational lakes and seawaters (Labille et al., 2020b; Gondikas et al., 2018), suggesting that hydrophobic TiO_2 NPs may undergo increased transport from their point of release, depending on environmental conditions (e.g., wind, flow). From an exposure perspective, the higher environmental concentrations of UV filters expected to be floating at the surface of recreational waters could lead to a higher associated risk if they come into contact with living organisms.

Conversely, the hydrophilic T-SiO_2 NPs were shown to immediately disperse in both the fresh- and seawater and were unstable in the water column, with rapid salt-induced homo-aggregation and complete sedimentation within 48 h. Thus, the 400 mg of hydrophilic TiO_2 NPs released from a single bather into freshwater or seawater would disperse completely and eventually deposit in the sediment (Fig. 3). In natural aqueous environments, the residence time of hydrophilic TiO_2 NPs in the water column is likely to be even shorter due to hetero-aggregation with natural suspended matter and subsequent sedimentation (Slomberg et al., 2019; Adam et al., 2016; Labille et al., 2015). The estimated mass flow of hydrophobic and hydrophilic TiO_2 NPs in ultrapure water is also shown in Fig. 3 to represent the possible fate in waters with low salinity. While the mass flow of the hydrophobic NPs would be minimally impacted, ~172 mg of the hydrophilic NPs could remain stable in the water column instead of sedimenting, potentially changing the exposure scenario.

3.4. Aging can impact particle coating integrity

The physical fate of the nanoparticulate UV filters in the water column is an important consideration for potential exposure, but the evaluation of aqueous aging of the TiO_2 particle coating(s), especially the photopassivation layer, is also crucial for determining any potential environmental effects and evaluating risk. While the stability of the T-SA stearic acid coating during aging was not explored in this work, 88–99% of the T-SA remained in the oil phase layer, suggesting that the stearic acid coating was retained. Significant loss of the stearic acid layer would have exposed the hydrophilic Al_2O_3 layer and promoted NP dispersion in the aqueous phase. In addition, stearic acid has previously been shown to be stable under UV irradiation in the absence of ROS generated from non-passivated, photoreactive TiO_2 (Mills and Wang, 2006). The stability of the Al_2O_3 photopassivation layer on the T-SA NPs was monitored indirectly by measuring dissolved Al (<2 nm) concentrations in the aqueous phase during the 48 h of aging. Since this coating represents 7.8 wt% of the T-SA NP composition, complete degradation of the Al_2O_3 layer and entry into the aqueous phase would result in a maximum Al concentration of ~12.8 mg/L. If degradation of the Al_2O_3 layer was only observed for the T-SA NPs present in the aqueous phase (~31 and 39 mg/L for the ultrapure and freshwater, respectively), maximum concentrations of ~1.3–1.6 mg/L Al would be expected after 48 h of aging. Over the course of the aqueous aging, no Al was detected (data not shown) under daylight conditions or in the dark in any of the aqueous systems (i.e., ultrapure water, freshwater, seawater) with ICP-AES (limit of quantification ~ 0.06 mg/L), signifying that the integrity of the Al_2O_3 photopassivation layer was retained.

For the case of T-SiO_2, previous work already demonstrated the significant degradation of the SiO_2 passivation layer after 48 h of aging and 48 h of settling in both freshwater and seawater (Slomberg et al., 2020b). However, an understanding of the kinetics of the SiO_2 layer dissolution was still lacking. As shown in Fig. 4A, the increase in dissolved Si (<2 nm) concentration in the aqueous

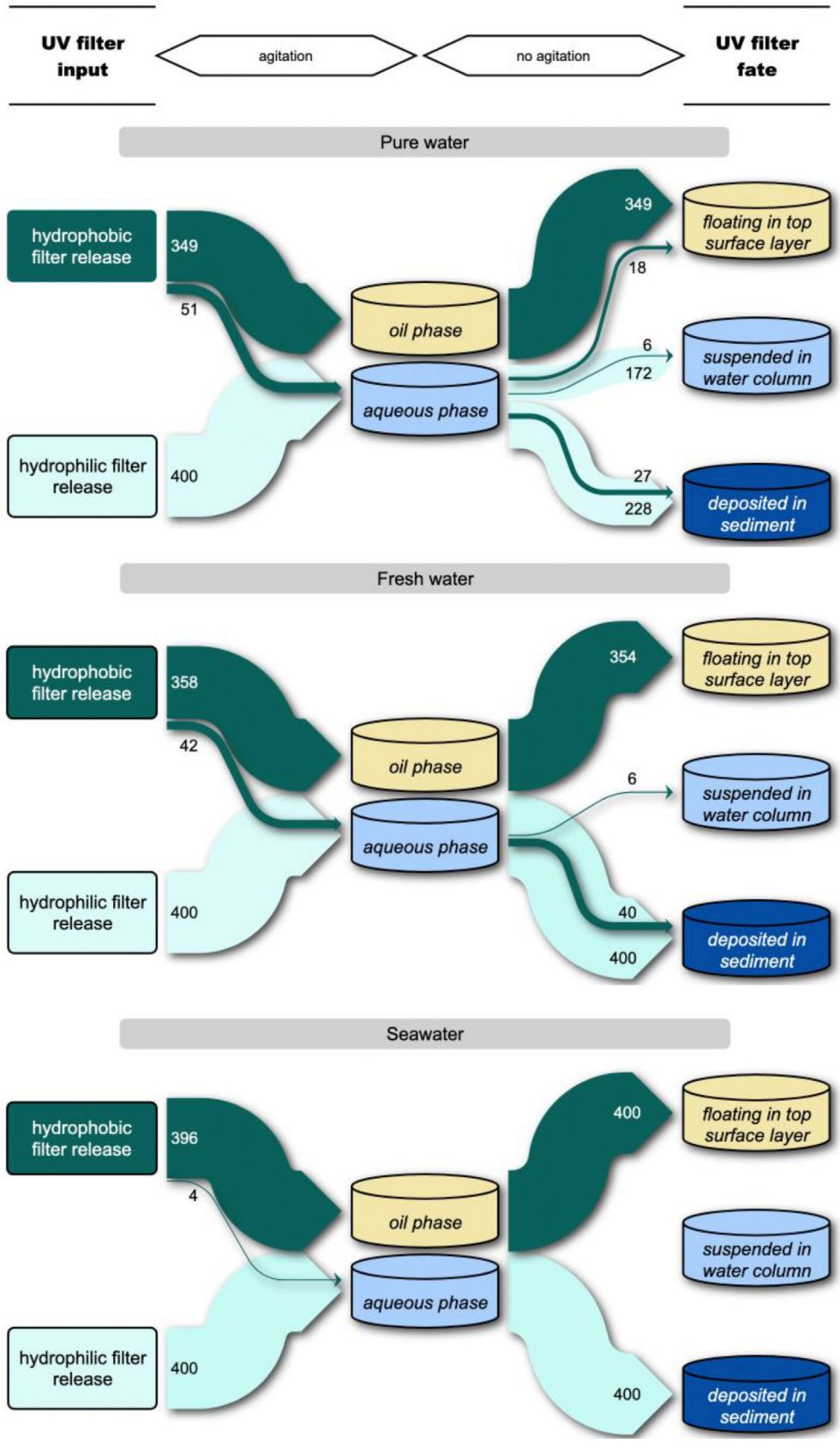

Fig. 3. Estimated mass flow (mg) of nanoparticulate TiO_2 UV filters (hydrophobic or hydrophilic) into ultrapure, freshwater, or seawater after release of 400 mg TiO_2 from a single bather following whole-body application of a 5% TiO_2 sunscreen.

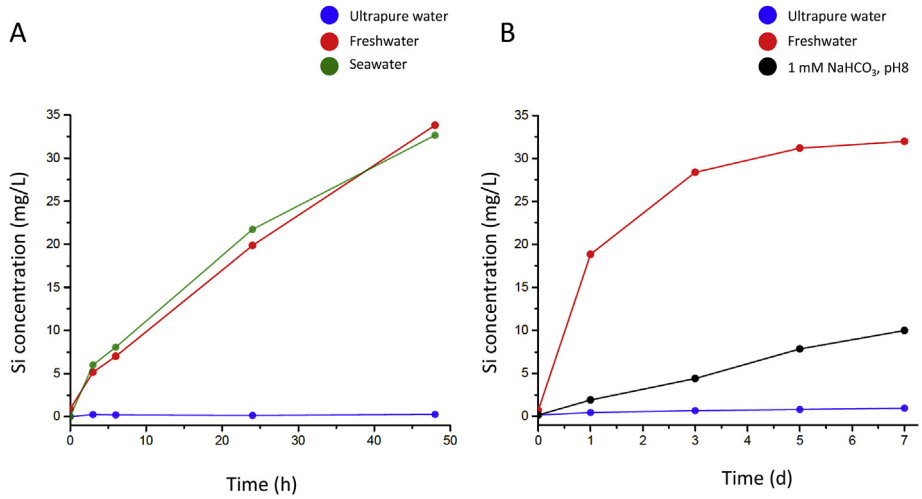

Fig. 4. Release of Si from T-SiO_2 coating into various aqueous solutions during aging A) under daylight conditions over 48 h and B) in dark over 7 days.

phase, indicating the loss of Si from the NP SiO_2 coating, was rapid in both the freshwater and seawater, with 5–6 mg/L Si measured in the aqueous phase at 3 h, representing a ~16–18% loss of the protective SiO_2 layer. The Si release from the T-SiO_2 nanocomposite into the fresh- and sea-waters continued as the aqueous aging progressed, with 19–21 mg/L Si (i.e., 61–66% SiO_2 coating degradation) present after 24 h. After 48 h of aging, the protective SiO_2 layer was almost completely degraded (99–100%), with ~30 mg/L Si measured in both the fresh- and sea-waters. However, in ultrapure water, the SiO_2 coating on the T-SiO_2 nanocomposite was stable, as no dissolved (<2 nm) Si was recovered in the aqueous phase over the 48 h of aging. These trends in Si release were not related to daylight exposure since the same trends were observed for T-SiO_2 NPs aged in the dark (Supplementary Material Figure S6).

To further examine the relationship between pH, ionic strength, and the duration of aging, the T-SiO_2 NPs were aged in freshwater (IS = 5.8 mM, pH 7.5), a lower ionic strength solution of 1 mM $NaHCO_3$ (pH 8), and ultrapure water (pH ~6), out to 7 days in the dark. As seen in Fig. 4B, after 7 days of aqueous aging in ultrapure water, some Si release (~1 mg/L) was observed, but this loss still only represented 3.1% of the SiO_2 coating. When the T-SiO_2 NPs were aged in the low ionic strength 1 mM $NaHCO_3$ solution at pH 8, a pH similar to the freshwater, the Si release was ~10 mg/L after 7 days, representing a coating loss of 32%. This was in contrast to the almost complete SiO_2 coating degradation in the freshwater and further supports an ionic strength accelerated dissolution mechanism as previously described in Slomberg et al. (2020b)

Zeta potential (ZP) measurements were performed on the pristine and aged T-SiO_2 materials to assess changes in the isoelectric point (IEP) related to any transformation of the particle coating (Supplementary Material Table S2). Under the tested pH conditions (pH 2–6), the pristine T-SiO_2 zeta potential remained negative (−16.5 to −36.6 mV), never reaching 0 mV, and thus signifying an IEP less than pH 2. In contrast, the IEP of the rutile TiO_2 core was between pH 4–6, which was consistent for IEP values previously determined for SiO_2 and rutile TiO_2 materials, respectively (Kim and Lawler, 2005; Ilina et al., 2017). The NPs aged in ultrapure (UP) water and recovered in the aqueous phase or in the sediment still retained some SiO_2 character and an IEP less than pH 2, with ZP values (pH 2) of −1.1 and −7.2 mV, respectively. However in the fresh- and sea-waters, with the loss of the SiO_2 coating, the NPs had more of the TiO_2 surface exposed and the IEP was between pH 2 and 4. These zeta potential measurements corroborate the degradation and instability of the SiO_2 coating revealed via elemental analysis.

3.5. Loss of coating leaves behind photoactive by-products

During aqueous aging, the T-SA NP Al_2O_3 photopassivation layer was retained under all tested conditions. As Al-based coatings (e.g., $Al(OH)_3$ and Al_2O_3) on TiO_2 NPs have already been shown to effectively inhibit ROS generation (Jang et al., 2016; Auffan et al., 2010), no further investigations on the photoreactivity of the aged T-SA NP UV filters were carried out. However, with the removal of the SiO_2 photopassivation layer from the T-SiO_2 NPs aged in simulated fresh- and seawater, it is likely that the exposed TiO_2 NP core would lead to photoactive by-products. A rhodamine degradation test was thus performed to evaluate the potential for various bare and coated TiO_2 NPs to form photoactive species upon exposure to daylight as shown in Fig. 5. In the absence of TiO_2 NPs, the rhodamine was mostly stable under daylight conditions, with ~14% degradation observed after 240 min. The photoactive, uncoated P25 TiO_2 NPs were used as a positive control, and as expected, the rhodamine was almost completely degraded within 90 min. In contrast, the uncoated 100% rutile NanoAmor TiO_2 NPs were less photoactive compared to the P25, with ~48% rhodamine

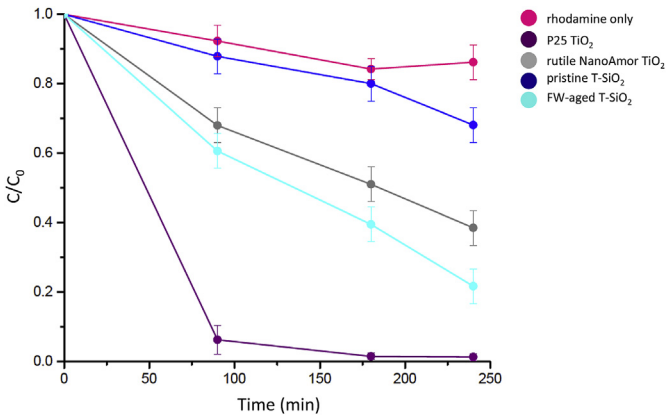

Fig. 5. Photocatalytic degradation curve of rhodamine solution in the presence of photoreactive P25 TiO_2, rutile NanoAmor TiO_2, pristine T-SiO_2, and freshwater (FW)-aged T-SiO_2 under daylight conditions.

degradation from TiO_2-induced ROS generation after 240 min. When a SiO_2 passivation coating was present on the rutile TiO_2, as was the case for the pristine T-SiO_2 NPs, the TiO_2-induced photoactivity was significantly inhibited, with rhodamine degradation reduced to ~18%. However, after this T-SiO_2 NP was aged in simulated freshwater and ~99% of the SiO_2 coating was removed, up to 65% of the rhodamine was degraded, with kinetics comparable to those observed for the bare 100% rutile NanoAmor TiO_2. The FW-aged T-SiO_2 even exhibited increased rhodamine degradation compared to the bare rutile NanoAmor TiO_2, likely due to slightly more ROS generation from the high aspect ratio, rod-shaped T-SiO_2 NPs compared to the spherical NanoAmor TiO_2 NPs (Dufour et al., 2015; Yun et al., 2009; Ali Ahmad et al., 2012). These results suggest that T-SiO_2 NPs released into fresh- and seawaters will not only lose their protective SiO_2 coating, but will also become photoactive, capable of generating ROS that may have detrimental impacts on a variety of biota, including coral reefs (Sendra et al., 2017a; Miller et al., 2012).

4. Conclusions

This work compared the fate and transformation of two nanoparticulate TiO_2 UV filters with different surface coatings (i.e., Al_2O_3/stearic acid or SiO_2) dispersed in their respective sunscreen phase (i.e., oil or water) upon release into ultrapure and simulated freshwater and seawater. The differences in water column residence time between the hydrophobic and hydrophilic TiO_2 UV filters suggest that the type of organisms (i.e., surface versus benthic) exposed may vary based on the TiO_2 surface coating and should be further explored. In addition to exposure considerations, understanding the transformation of the UV filter nanocomposite is also critical for assessing environmental impacts, as it could change the NP photoreactivity as well as bioavailability (Auffan et al., 2010; Fouqueray et al., 2012). The primary Al_2O_3 photopassivation layer on the T-SA NPs was resistant to aging in abiotic, simulated freshwater and seawater, indicating that this coating shows promise for preventing TiO_2 phototoxicity in aqueous environments. However, future work should confirm the resistance of the Al_2O_3 layer over a longer time period (i.e., >48 h) and in natural surface waters, as the presence of biota, such as microorganisms, may enhance aging. The resistance of the secondary stearic acid coating to aqueous aging was not within the scope of this work, but should also be considered in future studies as its removal would change the NP fate and bioavailability. In contrast, the SiO_2 coating on the T-SiO_2 NPs rapidly dissolved during aqueous aging, leaving behind a photoactive TiO_2 core that could lead to phototoxicity. Furthermore, in natural aqueous environments, the aged, photoactive T-SiO_2 NPs will readily aggregate and settle, potentially attaching to fragile organisms such as reefs. Future work should aim to further understand the toxicity of these aged nanoparticulate UV filters, using the results to improve material design and develop sunscreens that are more environmentally safe throughout their entire life-cycle.

Author statement

Danielle L. Slomberg: Conceptualization, Methodology, Investigation, Writing – original draft, Visualization, Supervision, Project administration. Riccardo Catalano: Investigation. Vincent Bartolomei: Investigation. Jérôme Labille: Funding acquisition, Conceptualization, Writing – original draft, Visualization, Project administration. All authors contributed to the article and approved the submitted version.

Declaration of competing interest

The authors declare that they have no known competing financial interests or personal relationships that could have appeared to influence the work reported in this paper.

Acknowledgements

This work is a contribution to the OSU-Institut Pytheas and to the Labex Serenade program (no. ANR-11-LABX-0064) funded by the "Investissements d'Avenir" program of the French National Research Agency (ANR) through the A*MIDEX project (no. ANR-11-IDEX-0001-02). We thank Jean-Claude Hubaud of Helioscience (Marseille, France) and Alexandra Lopes of Laboratoire CNB (Marseille, France) for their advice on the selection of TiO_2 UV filters and the oil phase formulation for this study.

Appendix A. Supplementary data

Supplementary data to this article can be found online at https://doi.org/10.1016/j.envpol.2020.116263.

References

Aarthi, T., Madras, G., 2007. Photocatalytic degradation of rhodamine dyes with nano- TiO_2. Ind. Eng. Chem. Res. 46, 7–14.
Adam, V., Loyaux-Lawniczak, S., Labille, J., Galindo, C., del Nero, M., Gangloff, S., Weber, T., Quaranta, G., 2016. Aggregation behaviour of TiO_2 nanoparticles in natural river water. J. Nanopart. Res. 18, 13.
Ali Ahmad, M., Prelot, B., Razafitianamaharavo, A., Douillard, J.M., Zajac, J., Dufour, F., Durupthy, O., Chaneac, C., Villiéras, F., 2012. Influence of morphology and crystallinity on surface reactivity of nanosized anatase TiO_2 studied by adsorption techniques. 1. The use of gaseous molecular probes. J. Phys. Chem. C 116, 24596–24606.
André, V., Willenbacher, N., Debus, H., Börger, L., Fernandez, P., Frechen, T., Rieger, J., 2003. Prediction of emulsion stability: facts and myth. Cosmet. Toiletries Manufact. Worldwide 102.
Auffan, M., Pedeutour, M., Rose, J., Masion, A., Ziarelli, F., Borschneck, D., Chanéac, C., Botta, C., Chaurand, P., Labille, J., Bottero, J.Y., 2010. Structural degradation at the surface of a TiO_2-based nanomaterial used in cosmetics. Environ. Sci. Technol. 44, 2689–2694.
Balmer, M.E., Buser, H.-R., Müller, M.D., Poiger, T., 2005. Occurrence of some organic UV filters in wastewater, in surface waters, and in fish from Swiss lakes. Environ. Sci. Technol. 39, 953–962.
Binks, B.P., Murakami, R., Armes, S.P., Fujii, S., 2006. Effects of pH and salt concentration on oil-in-water emulsions stabilized solely by nanocomposite microgel particles. Langmuir 22, 2050–2057.
Botta, C., Labille, J., Auffan, M., Borschneck, D., Miche, H., Cabié, M., Masion, A., Rose, J., Bottero, J.-Y., 2011. TiO_2-based nanoparticles released in water from commercialized sunscreens in a life-cycle perspective: structures and quantities. Environ. Pollut. 159, 1543–1550.
Catalano, R., Masion, A., Ziarelli, F., Slomberg, D., Laisney, J., Unrine, J.M., Campos, A., Labille, J., 2020. Optimizing the dispersion of nanoparticulate TiO2- based UV filters in a non-polar medium used in sunscreen formulations—The roles of surfactants and particle coatings. Colloids Surf. A: Physicochem. Eng. Asp. 599, 124792.
Catalano, R., Labille, J., Gaglio, D., Alijagic, A., Napodano, E., Slomberg, D., Campos, A., Pinsino, A., 2020. Safety evaluation of TiO_2 nanoparticle-based sunscreen UV filters on the development and the immunological state of the sea urchin *Paracentrotus lividus*. Nanomaterials 10, 2102.
Couteau, C., Coiffard, L., 2015. The interest in nanomaterials for topical photoprotection. Cosmetics 2, 394–408.
Couteau, C., Alami, S., Guitton, M., Paparis, E., Coiffard, L., 2008. Mineral filters in sunscreen products—comparison of the efficacy of zinc oxide and titanium dioxide by in vitro method. Die Pharmazie-An Int. J. Pharm. Sci. 63, 58–60.
Danovaro, R., Bongiorni, L., Corinaldesi, C., Giovannelli, D., Damiani, E., Astolfi, P., Greci, L., Pusceddu, A., 2008. Sunscreens cause coral bleaching by promoting viral infections. Environ. Health Perspect. 116, 441–447.
DiNardo, J.C., Downs, C.A., 2018. Dermatological and environmental toxicological impact of the sunscreen ingredient oxybenzone/benzophenone-3. J. Cosmet. Dermatol. 17, 15–19.
Dufour, F., Pigeot-Remy, S., Durupthy, O., Cassaignon, S., Ruaux, V., Torelli, S., Mariey, L., Maugé, F., Chanéac, C., 2015. Morphological control of TiO2 anatase nanoparticles: what is the good surface property to obtain efficient photocatalysts? Applied Catalysis B: Environmental, 174, 350–360.
Faure, B., Salazar-Alvarez, G., Ahniyaz, A., Villaluenga, I., Berriozabal, G., De Miguel, Y.R., Bergström, L., 2013. Dispersion and surface functionalization of

oxide nanoparticles for transparent photocatalytic and UV-protecting coatings and sunscreens. Sci. Technol. Adv. Mater. 14, 023001.
Ficheux, A., Chevillotte, G., Wesolek, N., Morisset, T., Dornic, N., Bernard, A., Bertho, A., Romanet, A., Leroy, L., Mercat, A., 2016. Consumption of cosmetic products by the French population second part: amount data. Food Chem. Toxicol. 90, 130–141.
Fouqueray, M., Dufils, B., Vollat, B., Chaurand, P., Botta, C., Abacci, K., Labille, J., Rose, J., Garric, J., 2012. Effects of aged TiO_2 nanomaterial from sunscreen on Daphnia magna exposed by dietary route. Environ. Pollut. 163, 55–61.
Fujishima, A., Zhang, X., Tryk, D.A., 2008. TiO_2 photocatalysis and related surface phenomena. Surf. Sci. Rep. 63, 515–582.
Fundin, J., Brown, W., Vethamuthu, M.S., 1996. Poly ((N, N, N-trimethylammonio) ethyl acrylate chloride salt)(PCMA)–SDS complex formation in dilute aqueous solution. Light scattering and time-resolved fluorescence quenching measurements. Macromolecules 1996 (29), 1195–1203.
Gago-Ferrero, P., Diaz-Cruz, M.S., Barceló, D., 2012. An overview of UV-absorbing compounds (organic UV filters) in aquatic biota. Anal. Bioanal. Chem. 404, 2597–2610.
Gondikas, A.P., von der Kammer, F., Reed, R.B., Wagner, S., Ranville, J.F., Hofmann, T., 2014. Release of TiO_2 nanoparticles from sunscreens into surface waters: a one-year survey at the old Danube recreational Lake. Environ. Sci. Technol. 48, 5415–5422.
Gondikas, A., von der Kammer, F., Kaegi, R., Borovinskaya, O., Neubauer, E., Navratilova, J., Praetorius, A., Cornelis, G., Hofmann, T., 2018. Where is the nano? Analytical approaches for the detection and quantification of TiO_2 engineered nanoparticles in surface waters. Environ. Sci.: Nano 5, 313–326.
Hanigan, D., Truong, L., Schoepf, J., Nosaka, T., Mulchandani, A., Tanguay, R.L., Westerhoff, P., 2018. Trade-offs in ecosystem impacts from nanomaterial versus organic chemical ultraviolet filters in sunscreens. Water Res. 139, 281–290.
Hsiung, C.-E., Lien, H.-L., Galliano, A.E., Yeh, C.-S., Shih, Y.-H., 2016. Effects of water chemistry on the destabilization and sedimentation of commercial TiO_2 nanoparticles: role of double-layer compression and charge neutralization. Chemosphere 151, 145–151.
Ilina, S.M., Ollivier, P., Slomberg, D., Baran, N., Pariat, A., Devau, N., Sani- Kast, N., Scheringer, M., Labille, J., 2017. Investigations into titanium dioxide nanoparticle and pesticide interactions in aqueous environments. Environ. Sci.: Nano 4, 2055–2065.
Jang, E., Sridharan, K., Park, Y.M., Park, T.J., 2016. Eliminated phototoxicity of TiO_2 particles by an atomic-layer-deposited Al_2O_3 coating layer for UV-protection applications. Chem. Eur. J. 22, 12022–12026.
Keller, A.A., Wang, H., Zhou, D., Lenihan, H.S., Cherr, G., Cardinale, B.J., Miller, R., Ji, Z., 2010. Stability and aggregation of metal oxide nanoparticles in natural aqueous matrices. Environ. Sci. Technol. 44, 1962–1967.
Kim, J.-K., Lawler, D.F., 2005. Characteristics of zeta potential distribution in silica particles. Bull. Kor. Chem. Soc. 26, 1083–1089.
King, D.M., Liang, X., Burton, B.B., Akhtar, M.K., Weimer, A.W., 2008. Passivation of pigment-grade TiO_2 particles by nano thick atomic layer deposited SiO2 films. Nanotechnology 19, 255604.
Kumar, J., Bansal, A., 2013. A comparative study of immobilization techniques for photocatalytic degradation of rhodamine B using nanoparticles of titanium dioxide. Water Air Soil Pollut. 224, 1452.
Labille, J., Feng, J., Botta, C., Borschneck, D., Sammut, M., Cabie, M., Auffan, M., Rose, J., Bottero, J.-Y., 2010. Aging of TiO_2 nanocomposites used in sunscreen. Dispersion and fate of the degradation products in aqueous environment. Environ. Pollut. 158, 3482–3489.
Labille, J., Harns, C., Bottero, J.-Y., Brant, J., 2015. Heteroaggregation of titanium dioxide nanoparticles with natural clay colloids under environmentally relevant conditions. Environ. Sci. Technol. 49, 6608–6616.
Labille, J., Catalano, R., Slomberg, D., Motellier, S., Pinsino, A., Hennebert, P., Santaella, C., Bartolomei, V., 2020. Assessing sunscreen lifecycle to minimize environmental risk posed by nanoparticulate UV-filters – a review for safer-by-design products. Front. Environ. Sci. 8.
Labille, J., Slomberg, D., Catalano, R., Robert, S., Apers-Tremelo, M.-L., Boudenne, J.-L., Manasfi, T., Radakovitch, O., 2020. Assessing UV filter inputs into beach waters during recreational activity: a field study of three French Mediterranean beaches from consumer survey to water analysis. Sci. Total Environ. 706, 136010.
Lewicka, Z.A., Benedetto, A.F., Benoit, D.N., William, W.Y., Fortner, J.D., Colvin, V.L., 2011. The structure, composition, and dimensions of TiO_2 and ZnO nanomaterials in commercial sunscreens. J. Nanopart. Res. 13, 3607.
Lewicka, Z.A., William, W.Y., Oliva, B.L., Contreras, E.Q., Colvin, V.L., 2013. Photochemical behavior of nanoscale TiO_2 and ZnO sunscreen ingredients. J. Photochem. Photobiol. A Chem. 263, 24–33.
Li, Y., Zhang, W., Niu, J., Chen, Y., 2012. Mechanism of photogenerated reactive oxygen species and correlation with the antibacterial properties of engineered metal- oxide nanoparticles. ACS Nano 6, 5164–5173.
Loosli, F., Stoll, S., 2017. Effect of surfactants, pH and water hardness on the surface properties and agglomeration behavior of engineered TiO_2 nanoparticles. Environ. Sci.: Nano 4, 203–211.
Loosli, F., Wang, J., Rothenberg, S., Bizimis, M., Winkler, C., Borovinskaya, O., Flamigni, L., Baalousha, M., 2019. Sewage spills are a major source of titanium dioxide engineered (nano)-particle release into the environment. Environ. Sci.: Nano 6, 763–777.
Marti-Mestres, G., Fernandez, C., Parsotam, N., Nielloud, F., Mestres, J., Maillols, H., 1997. Stability of UV filters in different vehicles: solvents and emulsions. Drug Dev. Ind. Pharm. 23, 647–655.
Matta, M.K., Zusterzeel, R., Pilli, N.R., Patel, V., Volpe, D.A., Florian, J., Oh, L., Bashaw, E., Zineh, I., Sanabria, C., 2019. Effect of sunscreen application under maximal use conditions on plasma concentration of sunscreen active ingredients: a randomized clinical trial. J. Am. Med. Assoc. 321, 2082–2091.
Matta, M.K., Florian, J., Zusterzeel, R., Pilli, N.R., Patel, V., Volpe, D.A., Yang, Y., Oh, L., Bashaw, E., Zineh, I., 2020. Effect of sunscreen application on plasma concentration of sunscreen active ingredients: a randomized clinical trial. J. Am. Med. Assoc. 323, 256–267.
Metin, C.O., Lake, L.W., Miranda, C.R., Nguyen, Q.P., 2011. Stability of aqueous silica nanoparticle dispersions. J. Nanopart. Res. 13, 839–850.
Miller, R.J., Bennett, S., Keller, A.A., Pease, S., Lenihan, H.S., 2012. TiO_2 nanoparticles are phototoxic to marine phytoplankton. PloS One 7, e30321.
Mills, A., Wang, J., 2006. Simultaneous monitoring of the destruction of stearic acid and generation of carbon dioxide by self-cleaning semiconductor photocatalytic films. J. Photochem. Photobiol. A: Chem. 182, 181–186.
Mya, K.Y., Sirivat, A., Jamieson, A.M., 2003. Effect of ionic strength on the structure of polymer–surfactant complexes. J. Phys. Chem. B 107, 5460–5466.
Narla, S., Lim, H.W., 2020. Sunscreen: FDA regulation, and environmental and health impact. Photochem. Photobiol. Sci. 19, 66–70.
Park, B.J., Pantina, J.P., Furst, E.M., Oettel, M., Reynaert, S., Vermant, J., 2008. Direct measurements of the effects of salt and surfactant on interaction forces between colloidal particles at water–oil interfaces. Langmuir 24, 1686–1694.
Praetorius, A., Labille, J., Scheringer, M., Thill, A., Hungerbühler, K., Bottero, J.-Y., 2014. Heteroaggregation of titanium dioxide nanoparticles with model natural colloids under environmentally relevant conditions. Environ. Sci. Technol. 48, 10690–10698.
Ramalho, J., Marques, N., Semedo, J., Matos, M., Quartin, V., 2002. Photosynthetic performance and pigment composition of leaves from two tropical species is determined by light quality. Plant Biol. 4, 112–120.
Rand, L.N., Bi, Y., Poustie, A., Bednar, A.J., Hanigan, D.J., Westerhoff, P., Ranville, J.F., 2020. Quantifying temporal and geographic variation in sunscreen and mineralogic titanium-containing nanoparticles in three recreational rivers. Sci. Total Environ. 743, 1, 40845.
Reed, R., Martin, D., Bednar, A., Montaño, M., Westerhoff, P., Ranville, J., 2017. Multi-day diurnal measurements of Ti-containing nanoparticle and organic sunscreen chemical release during recreational use of a natural surface water. Environ. Sci.: Nano 4, 69–77.
Rodríguez-Romero, A., Ruiz-Gutiérrez, G., Viguri, J.R., Tovar-Sánchez, A., 2019. Sunscreens as a new source of metals and nutrients to coastal waters. Environ. Sci. Technol. 53, 10177–10187.
Romanhole, R.C., Ataide, J.A., Cefali, L.C., Moriel, P., Mazzola, P.G., 2016. Photostability study of commercial sunscreens submitted to artificial UV irradiation and/or fluorescent radiation. J. Photochem. Photobiol. B Biol. 162, 45–49.
SCCS, 2012. OPINION ON Zinc Oxide (nano form). COLIPA S76. Scientific Committee on Consumer Safety, Brussels.
SCCS, 2014. OPINION ON Titanium Dioxide (nano form). COLIPA S75. Scientific Committee on Consumer Safety, Brussels.
Schlumpf, M., Schmid, P., Durrer, S., Conscience, M., Maerkel, K., Henseler, M., Gruetter, M., Herzog, I., Reolon, S., Ceccatelli, R., 2004. Endocrine activity and developmental toxicity of cosmetic UV filters—an update. Toxicology 205, 113–122.
Schneider, S.L., Lim, H.W., 2019. Review of environmental effects of oxybenzone and other sunscreen active ingredients. J. Am. Acad. Dermatol. 80, 266–271.
Schneider, S.L., Lim, H.W., 2019. A review of inorganic UV filters zinc oxide and titanium dioxide. Photodermatol. Photoimmunol. Photomed. 35, 442–446.
Semenzato, A., Dall'Aglio, C., Boscarini, G., Ongaro, A., Bettero, A., Sangalli, M., Brunetta, F., 1994. Chemico-physical and functional properties of inorganic sunscreens in cosmetic products. Int. J. Cosmet. Sci. 16, 247–255.
Sendra, M., Sánchez-Quiles, D., Blasco, J., Moreno-Garrido, I., Lubián, L.M., Perez-Garcia, S., Tovar-Sánchez, A., 2017. Effects of TiO_2 nanoparticles and sunscreens on coastal marine microalgae: ultraviolet radiation is key variable for toxicity assessment. Environ. Int. 98, 62–68.
Sendra, M., Moreno-Garrido, I., Yeste, M.P., Gatica, J.M., Blasco, J., 2017. Toxicity of TiO_2, in nanoparticle or bulk form to freshwater and marine microalgae under visible light and UV-A radiation. Environ. Pollut. 227, 39–48.
Skoglund, S., Lowe, T.A., Hedberg, J., Blomberg, E., Wallinder, I.O., Wold, S., Lundin, M., 2013. Effect of laundry surfactants on surface charge and colloidal stability of silver nanoparticles. Langmuir 29, 8882–8891.
Slomberg, D.L., Ollivier, P., Miche, H., Angeletti, B., Bruchet, A., Philibert, M., Brant, J., Labille, J., 2019. Nanoparticle stability in lake water shaped by natural organic matter properties and presence of particulate matter. Sci. Total Environ. 656, 338–346.
Slomberg, D.L., Auffan, M., Guéniche, N., Angeletti, B., Campos, A., Borschneck, D., Aguerre-Chariol, O., Rose, J., 2020. Anthropogenic release and distribution of titanium dioxide particles in a river downstream of a nanomaterial manufacturer industrial site. Front. Environ. Sci. 8.
Slomberg, D.L., Catalano, R., Ziarelli, F., Viel, S., Bartolomei, V., Labille, J., Masion, A., 2020. Aqueous aging of a silica coated TiO_2 UV filter used in sunscreens: investigations at the molecular scale with dynamic nuclear polarization NMR. RSC Adv. 10, 8266–8274.
Smijs, T.G., Pavel, S., 2011. Titanium dioxide and zinc oxide nanoparticles in sunscreens: focus on their safety and effectiveness. Nanotechnol. Sci. Appl. 4, 95.
Thiagarajan, V., Iswarya, V., Seenivasan, R., Chandrasekaran, N., Mukherjee, A., 2019. Influence of differently functionalized polystyrene microplastics on the toxic

effects of P25 TiO_2 NPs towards marine algae *Chlorella sp*. Aquat. Toxicol. 207, 208–216.
Topuz, E., Sigg, L., Talinli, I., 2014. A systematic evaluation of agglomeration of Ag and TiO_2 nanoparticles under freshwater relevant conditions. Environ. Pollut. 193, 37–44.
Tovar-Sánchez, A., Sánchez-Quiles, D., Basterretxea, G., Benedé, J.L., Chisvert, A., Salvador, A., Moreno-Garrido, I., Blasco, J., 2013. Sunscreen products as emerging pollutants to coastal waters. PloS One 8, e65451.
Tovar-Sánchez, A., Sánchez-Quiles, D., Rodríguez-Romero, A., 2019. Massive coastal tourism influx to the Mediterranean Sea: the environmental risk of sunscreens. Sci. Total Environ. 656, 316–321.
U.S. EPA, 2010. Nanomaterial Case Studies: Nanoscale Titanium Dioxide in Water Treatment and in Topical Sunscreen (Final). U.S. Environmental Protection Agency, Washington D.C.. EPA/600/R-09/057F, 2010.
U.S. Food and Drug Administration, 2019. Sunscreen drug products for over-the-counter human use. Fed. Regist. 84, 6204–6275.
Yun, H.J., Lee, H., Joo, J.B., Kim, W., Yi, J., 2009. Influence of aspect ratio of TiO_2 nanorods on the photocatalytic decomposition of formic acid. J. Phys. Chem. C 113, 3050–3055.